Pergamon

NanoStructured Materials, Vol. 8, No. 1, pp. 1-17, 1997
Elsevier Science Ltd
Copyright © 1997 Acta Metallurgica Inc.
Printed in the USA. All rights reserved
0965-9773/97 $17.00 + .00

PII S0965-9773(97)00071-8

MICROWAVE PLASMA SYNTHESIS OF CARBON-SUPPORTED ULTRAFINE METAL PARTICLES

J.R. Brenner, J.B.L. Harkness, M.B. Knickelbein, G.K. Krumdick, and C.L. Marshall

Argonne National Laboratory, Chemistry and Energy Systems Divisions,
9700 S. Cass Ave., Argonne, IL 60439, USA

(Accepted December 1996)

Abstract *— Microwave plasma decomposition of metal carbonyls has been used to synthesize a series of carbon-supported monometallic (Fe, Co) and bimetallic (Co-Mo) materials. The average metal particle diameters in all cases were less than 10 nm. By using 10% H_2/Ar instead of pure Ar as a carrier gas, the mean particle diameters could be decreased to less than 2 nm. Although the distribution of particles is slightly broader than those generated by other nanoparticle synthesis methods, the mean diameter of the particles generated using 10% H_2/Ar is as small as any previously reported for Fe-, Co-, Ni-, or Mo-containing compounds. The ultrafine metal particles were dispersed on moderate surface area amorphous carbon support matrixes derived from the concomitant microwave decomposition of the toluene solvent.*

INTRODUCTION

Though the preparation of highly dispersed, supported metal catalysts has received considerable attention, it has remained an area of active interest. Typically, metal-containing heterogeneous catalysts are prepared either by spray drying, incipient wetness impregnation of water-soluble metal precursors onto either an oxide (*e.g.* silica or alumina) or activated carbon support (1-3), or ion exchange into a zeolite support (4). While conventional methods are sufficient for the stabilization of noble metal particles (*e.g.* Rh, Pt) of less than 3 nm (5-12), the mean particle sizes of Group VIII first-row transition metals (Fe, Co, Ni) prepared by conventional methods typically are ≥ 4 nm (1-4).

The synthesis of ultrafine metal particles (d ≤ 50 nm) has not only been of interest to the catalysis community (13-23), but has attracted interest from groups interested in materials for magnetic storage (24-47) and electronics nanofabrication (48-51) as well. Methods used to synthesize metallic nanoparticles for magnetic storage and electronics nanofabrication vary widely, and include thermal dissociation of metal carbonyls (24-25, 49-50), laser-assisted dissociation of metal carbonyls (26-30, 48), evaporation of a metal target (31-37), colloidal growth of inverse micelles (38-40, 51), microwave plasma dissociation (31,41), and arc plasma evaporation (47). Several recent papers have described the use of laser pyrolysis (13-16, 23), inverse micelles (17-19), metal evaporation (21), and organometallic evaporation (20, 22) for the purpose

of making catalytic materials for coal liquefaction (13, 17-19), Fischer-Tropsch (14-16, 20), oxygen reduction (22), and ethane hydrogenolysis (23). With the exception of the ethane hydrogenolysis study, the catalytic materials produced by the aforementioned techniques were not as active as the commercial catalysts for those reactions. Interestingly, Pt particles generated by laser pyrolysis were reported to be sixty times more active for ethane hydrogenolysis than conventionally-prepared, supported Pt catalysts (23). Notably absent, however, is work describing the use of microwave plasma processing, an inexpensive alternative to laser light, to generate catalytic materials. In this paper, we report the preparation of first-row, Group VIII transition metal nanoparticles with mean diameters as small as 1.6 nm simultaneously with a carbonaceous support matrix using the microwave plasma-induced dissociation of organometallic precursors. The application of these materials as catalysts for the hydrodesulfurization of heavy crude oils will be described in a future paper.

EXPERIMENTAL

Materials and Methods

Reagent grade $Fe(CO)_5$, $Co_2(CO)_8$, and $Mo(CO)_6$, were obtained from Alfa. These organometallics were sprayed into a carrier gas upstream of the microwave plasma as saturated solutions in reagent grade toluene (Aldrich). The room temperature solubilities of $Co_2(CO)_8$ and $Mo(CO)_6$ in toluene was determined to be approximately 0.42 and 0.107 M, respectively. The $Fe(CO)_5$ was used both neat and as a 1:3 (mole fraction) solution in toluene. Aside from filtration immediately prior to use, the prepared reagents were used without further purification.

Hydrodesulfurization catalysts are typically composed of γ-Al_2O_3- or activated carbon-supported, bimetallic Co-Mo or Ni-Mo sulfides (1-3 wt.% Co or Ni as metal, 5-8% Mo as metal). Since one would expect that the entire toluene solution of metal carbonyls would be vaporized during microwave decomposition, a solution with a Mo:Co ratio of approximately 3:1 by metal weight was prepared (0.100 M $Mo(CO)_6$ and 0.027 M $Co_2(CO)_8$ dissolved in toluene). Table 1 lists the sample codes, metal carbonyl precursors, solvents, and carrier gases used to prepare the carbon-supported metal-containing materials.

TABLE 1
Preparation of Materials

Code	Precursors	Solvent	Carrier Gas
Fe/nosol/Ar	$Fe(CO)_5$	None	Ar
Fe/tol/Ar	$Fe(CO)_5$	Toluene	Ar
Co/tol/Ar	$Co_2(CO)_8$	Toluene	Ar
Co-Mo/tol/Ar	$Co_2(CO)_8$/$Mo(CO)_6$	Toluene	Ar
Co-Mo/tol/H_2-Ar	$Co_2(CO)_8$/$Mo(CO)_6$	Toluene	10% H_2/Ar

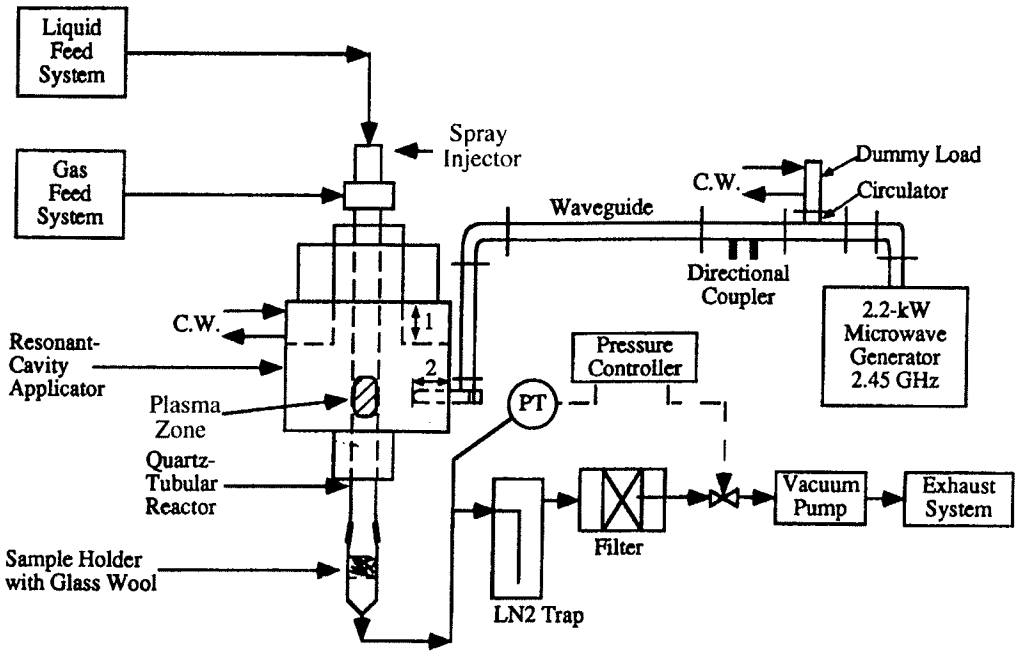

Figure 1. Schematic of microwave plasma dissociation apparatus.

The configuration of the apparatus used in these experiments is shown in Figure 1 (52-53). The gas-feed system used mass-flow controllers to meter the carrier gas, either Ar (AGA, 99.999%) or a mixture of 0.5 liter/min. H_2 (AGA, 99.999%) plus 4.5 liters/min. Ar (AGA, 99.999%), into a 35 mm o.d. cylindrical quartz reactor. A peristaltic pump metered the organometallic solution from a 50 ml burette to the top of the reactor, where it was sprayed into the carrier gas 45 cm above the plasma zone. The reactor extended past microwave chokes on both sides of the resonant-cavity applicator so that quartz was the only material exposed to either the microwave radiation or the plasma. The reactor operating pressure was 60 ± 5 torr (8.0 ± 0.7 kPa) in every experiment. In all these experiments, the system pressure was controlled by pressure transducer/controller that operates a throttling valve between the reactor and the main vacuum pump.

The microwave generator in these experiments was a continuously variable, 2.2-kW magnetron (2.45 GHz) operated at 500 W (measured by a directional coupler and a Hewlett Packard 435B power meter). The magnetron output was inserted into a tunable, resonant-cavity applicator (operated in the TE_{112} mode) with an adjustable launch probe connected to the magnetron by a rectangular waveguide. In order to protect the magnetron, reverse power was diverted to a dummy load by a water-cooled circulator.

At the reactor exit, a sample holder packed with glass wool was used to trap the particulate products of the plasma-chemical decomposition reactions. The sample holder containing the particulate products was sealed under flowing Ar with Parafilm and transferred within an hour to a N_2-purged glove box for later use.

Following the sample holder, the gas stream was passed through a LN_2 cold trap to collect both unreacted organometallics and organic byproducts. The noncondensibles were exhausted through a vacuum pump to the laboratory ventilation system.

Nitrogen Physisorption

Approximately 0.10 g of metal/carbon material was weighed into a Pyrex tube and evacuated at 80 mTorr for at least one hour. After backfilling with He, the supported metal was briefly exposed to air prior to analysis. The static physisorption experiments consisted of determining the amount of liquid N_2 adsorbing to or desorbing from the material as a function of pressure (P/P_o = 0.025-0.999, increments of 0.025) and were carried out using an Autosorb-6. Surface areas reported here are from the desorption isotherm.

Transmission Electron Microscopy

Approximately 0.01 g of carbon-supported metal was placed into a vial containing ~ 10 ml of isopropanol. After sonicating for 30 minutes, several drops of the resulting slurry were pipetted onto 3 mm holey carbon on Cu grids. Once dry, the grids were inserted into non-tilt holders and loaded into a JEOL 4000EX II (line-to-line resolution = 0.14 nm, point-to-point resolution = 0.17 nm). In many cases, regions not overhanging holes in the carbon grid were unsuitable. The micrographs were in all cases taken at magnifications of either 150,000x or 500,000x.

After scanning in the micrographs at 400 dpi using a Silverscan II scanner, the measuring tool function in NIH Image 1.59™ was used to determine the particle diameters. The distances have been referenced to those for the {002} planes of graphite (d_{002} = 0.338 nm., ref. 54), when present, examined at 500,000x and scanned in at 600 dpi. Diffraction patterns were obtained by Fourier transformation of selected particles using NIH Image 1.59™ to confirm phase and plane identification. The degree of accuracy (± 3%) was sufficient to make phase and plane identifications but was insufficient to detect any change in lattice parameter between the surface and bulk of the supported phase.

RESULTS

Synthesis Results

The duration of the experiments reported here was limited by the build-up of carbon on the inner wall of the quartz-tubular reactor which began to absorb microwave energy as this layer became conductive. This decreased the energy available for maintaining the plasma which, eventually, would extinguish. The growing carbon film also began to overheat the quartz, threatening tube failure. This limitation will be addressed in a subsequent design of the system to be described in future work.

Whereas 0.2-0.3 g of metal carbonyl in 8 g of toluene solution was fed into the microwave plasma, the amount of sample collected was never more than 0.1 g, and in several cases, only 0.02 g of material could be collected. The microwave plasma-generated material was deposited on both the walls of the quartz collection tube and on the Pyrex (or quartz wool). The bulk of the metal-on-carbon materials were deposited onto the wool but could not be separated from it. Therefore, all the material described in this paper was scraped off the outside walls of the quartz tube, in a

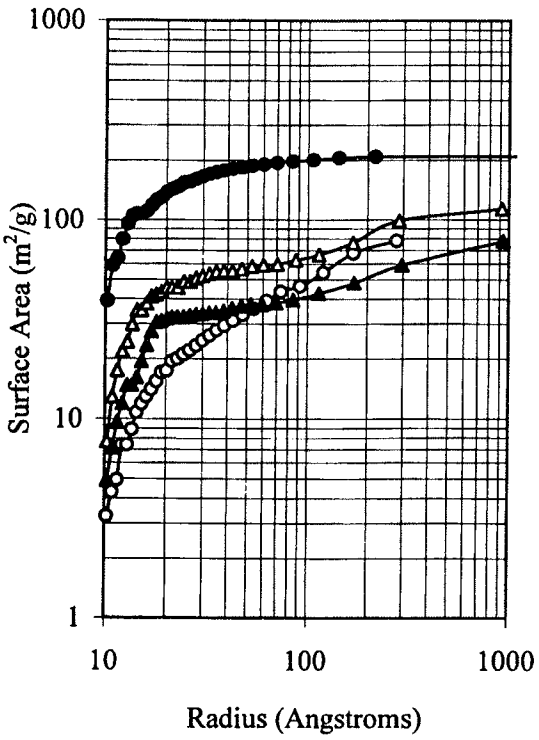

Figure 2. Cumulative surface areas of (o) Fe/tol/Ar, (Δ) Co/tol/Ar, (●) Co-Mo/tol/Ar, and (▲) Co- Mo/tol/H_2-Ar materials of the carbonaceous "supports" in the materials generated using toluene solvent. The Fe/nosol/Ar material, produced using $Fe(CO)_5$, had negligible surface area.

manner quite similar to those used for collection of fullerene soot. The purpose of the wool was to increase the effective surface area for metal particles deposition (and collection). In future work, we plan to deposit the metal particles directly onto a cordierite monolith similar to those used for automotive exhaust catalyst supports so that the metallic particles can be transferred directly to a catalytic testing unit.

Thus, in these experiments there was insufficient sample for analyses other than N_2 physisorption and TEM experiments. The sample for which the most material was collected was Fe/nosol/Ar, the only material for which no solvent was used. The dissociated toluene was not trapped out using LN_2; most likely it went to the exhaust as CH_4. Chou and Phillips (41) have also reported very low yields for microwave plasma-generated 10 nm Fe-containing particles, with much higher yields for 20-50 nm Fe-containing particles.

These materials were pyrophoric, suggesting that they initially had no oxide passivation layer. Two samples oxidized upon exposure to ambient air following nitrogen physisorption experiments. No such oxidation was observed visually during the transfer steps prior to storage in a N_2-filled glove box or prior to nitrogen physisorption and TEM experiments.

Nitrogen Physisorption

The pore volume of the Fe/nosol/Ar material was too low to be detected (< 0.001 cm^3/g). However, the materials prepared using toluene solvent produced isotherms which were convex to the P/P_o axis over its entire range and contained a slight amount of hysteresis. In addition, N_2 adsorption occurred in steps. Both the absence of an inflection point in the adsorption/desorption isotherms and the stepwise N_2 adsorption indicate that adsorbate-adsorbate interactions were stronger than adsorbate-adsorbent interactions. These results are consistent with the rare Type III isotherm (55) and previous work on both carbon blacks and graphites (56-58).

Figure 2 displays the cumulative surface areas from the desorption branches of the materials prepared using toluene solvent. The Fe/tol/Ar, Co/tol/Ar, and Co-Mo/tol/H_2-Ar materials had surface areas near 100 m^2/g and possessed nearly equal amounts of mesopores and macropores, with almost no micropores. In contrast, the Co-Mo/tol/Ar sample possessed a substantial micropore surface area (40 m^2/g), a large mesopore surface area (160 m^2/g), and almost no macropores.

Transmission Electron Microscopy

The Fe particles in the Fe/nosol/Ar product (Figure 3) were exceptionally uniform with a log mean particle size of 4.5 nm. By contrast, the Fe-containing particles in the Fe/tol/Ar product

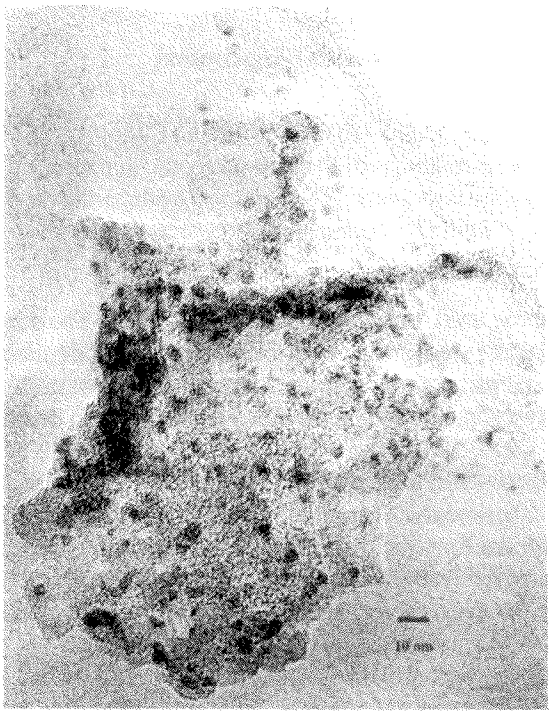

Figure 3. TEM micrograph of Fe/nosol/Ar.

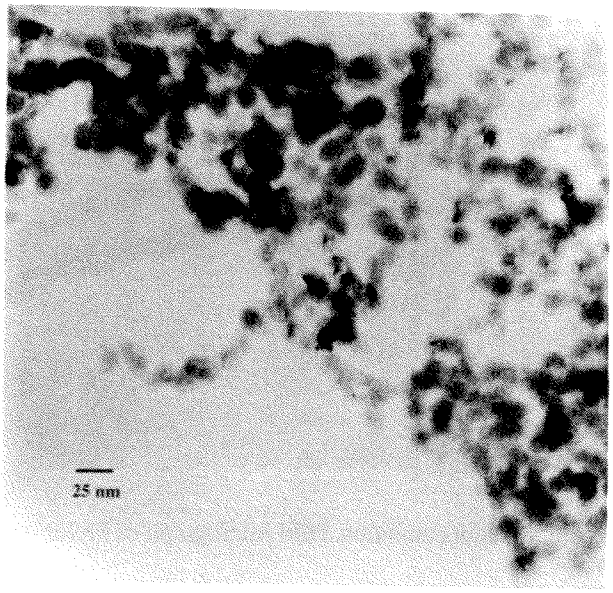

Figure 4. Low resolution TEM micrograph of Fe/tol/Ar.

(Figures 4 and 5) were much larger, including some which were faceted and consistent only with monoclinic Fe_2O_3 (d_{102} = 0.260 nm, d_{200} = 0.203 nm, ref. 59). These results show that the ultrafine particles were completely oxidized. The particles were certainly not oxidic prior to physisorption experiments, however, as evidenced by the fact that several samples displayed pyrophoricity following the physisorption experiments. These results suggest that the unpassivated particles oxidized during TEM sample preparation or transfer. The metal-containing particles from the Co/tol/Ar synthesis (Figure 6) were slightly smaller than those in Fe/tol/Ar and were consistent with hexagonal Co_2O_3 (d_{002} = 0.287 nm, ref. 60). The metal oxide particles were anchored to a largely amorphous carbon support matrix. Very few of the metal oxide particles were encapsulated by a graphitic overlayer. In fact, the Fe/tol/Ar material was the only one for which any graphite was observed (Figure 5).

The particles produced from the mixed Co-Mo in toluene solution (Figures 7 and 8) were in general far smaller than those in the monometallic materials. The addition of hydrogen to the argon carrier gas resulted, in general, in much smaller particles. In one region of the Co-Mo/tol/H_2-Ar material, however, the particles were far larger than in any of the other regions (~11 nm, Figure 9). This region was of marginal statistical significance. The only particles in either of the bimetallic materials for which the structure could be determined had a lattice spacing consistent only with monoclinic $CoMoO_4$ (d_{002} = 0.355 nm, ref. 61), suggesting a mixing of the two metals on the atomic scale. No graphitic material or evidence of encapsulation were present in either of the bimetallic materials.

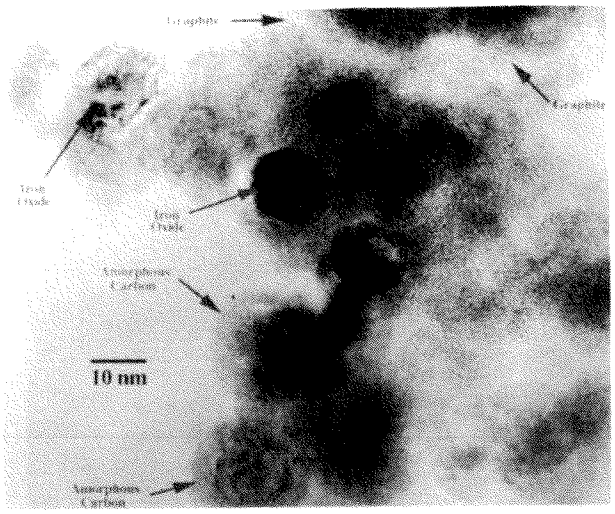

Figure 5. High resolution TEM micrograph of Fe/tol/Ar.

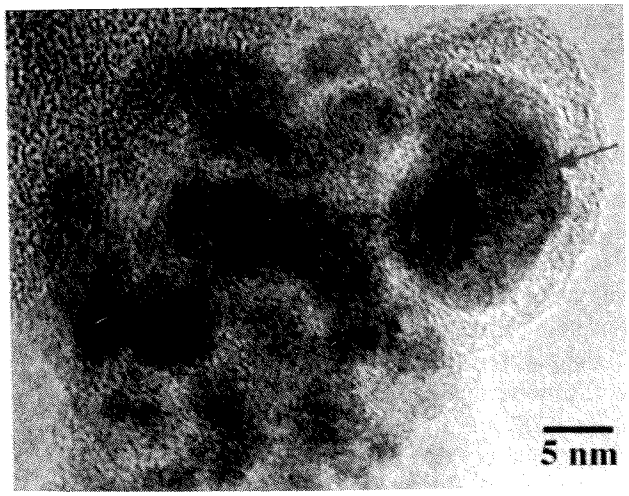

Figure 6. TEM Micrograph of Co/tol/Ar. An arrow indicates a particle of hexagonal Co_2O_3.

Particle size distributions were constructed by grouping the data into logarithmically evenly-spaced bins ranging from 0.17 nm to 100 nm (10 bins/factor of 10 change in diameter). The data were then fitted with either one or two log-normal distributions (Eqn. 1) using the commercially available program PeakFit (Jandel Scientific) where x is a given diameter, $f_{LN}(x)$ is the log-distributed probability density function, $\overline{x}$ is the log-mean diameter, and σ is the geometric standard deviation.

$$f_{LN}(x) = \frac{1}{(2\pi)^{0.5}\ln(\sigma)}\exp\left(\frac{-\left[\ln(x/\bar{x})\right]^2}{2\ln^2(\sigma)}\right) \qquad [1]$$

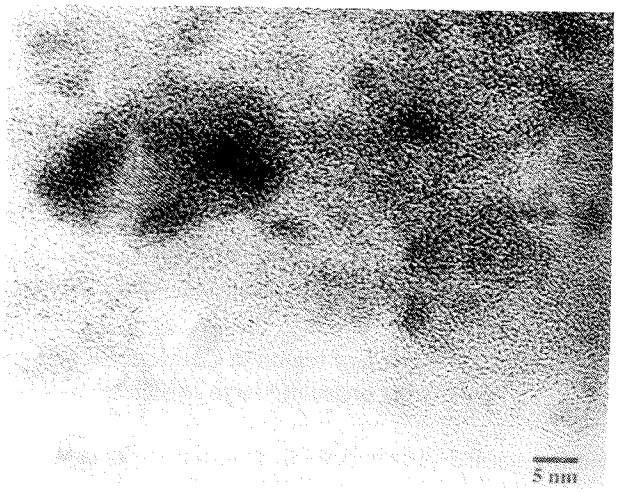

Figure 7. TEM micrograph of Co-Mo/tol/Ar.

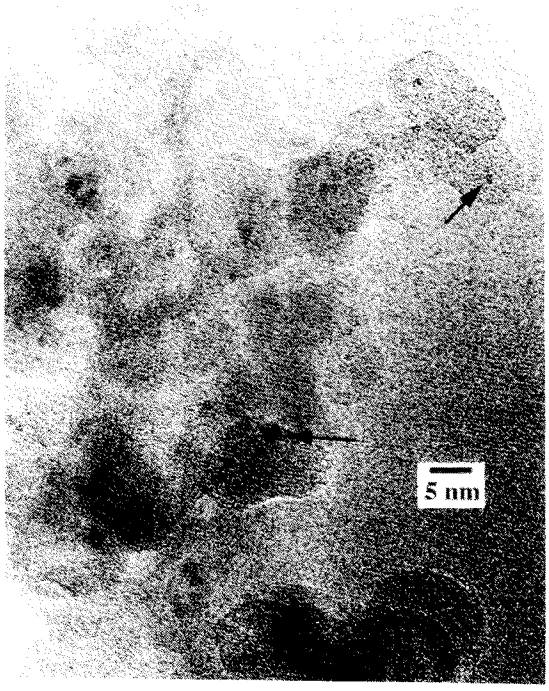

Figure 8. TEM micrograph of a typical region in Co-Mo/tol/H_2-Ar.

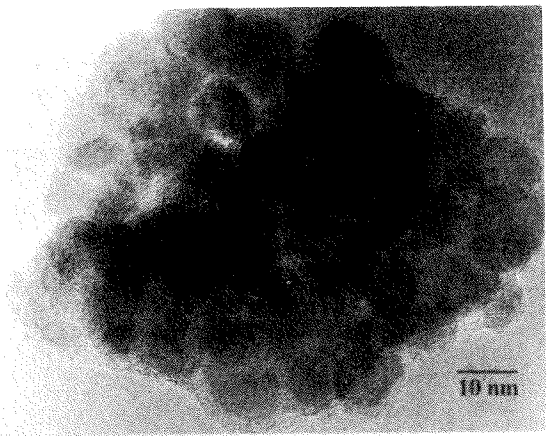

Figure 9. TEM micrograph of region in Co-Mo/tol/H_2-Ar material containing unusually large particles.

The use of two log-normal distributions to describe the data was avoided except when absolutely necessary. Granqvist and Buhrman (3) have shown that the log-normal particle size distribution can be predicted from coalescence theory and provides an excellent fit to particle size distribution data for spherical particles < 20 nm in diameter grown by a variety of methods.

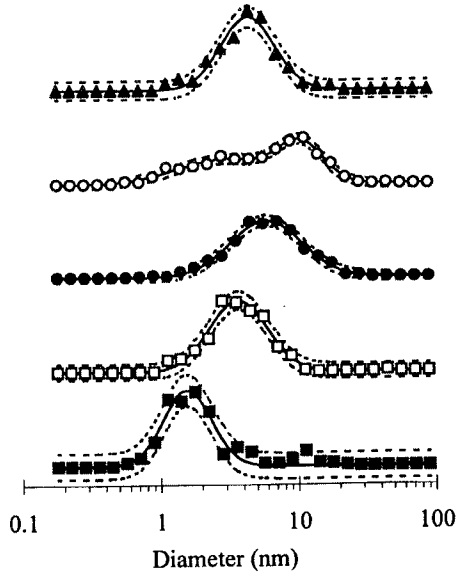

Figure 10. TEM particle size distributions of (▲) Fe/nosol/Ar, (o) Fe/tol/Ar, (●) Co/tol/Ar, (❑) Co-Mo/tol/Ar, and (■) Co-Mo/tol/H_2-Ar materials. The vertical axis is probability density on a linear scale, and the horizontal axis is particle diameter on a logarithmic scale. Solid and dashed curves indicate the data fits and 95% prediction intervals.

TABLE 2
Particle Size Distributions

Code	Log Mean(s) (nm)	G.S.D(s)*	Area %	# of Particles
Fe/nosol/Ar	4.5 ± 0.1	1.47 ± 0.02	100	170
Fe/tol/Ar	3.1 ± 0.4	1.96 ± 0.12	36	1029
	10.9 ± 0.3	1.39 ± 0.03	64	
Co/tol/Ar	6.0 ± 0.1	1.64 ± 0.02	100	328
Co-Mo/tol/Ar	3.7 ± 0.1	1.47 ± 0.05	100	272
Co-Mo/tol/H_2-Ar	1.56 ± 0.04	1.41 ± 0.03	100	405

Reported errors are standard deviations of the curve fit approximations to a given parameter.
*G.S.D = Geometric Standard Deviation = diameter corresponding to 84.13% probability divided by the log mean diameter.

Figure 10 displays the particle size distribution data (points), the computer fit of the data (solid line), and the 95% prediction intervals (dashed lines) for all the materials synthesized. This 95% prediction interval defines the confidence interval for an individual curve fit. Note that the abscissa of these histograms has been scaled logarithmically. The log means, geometric standard deviations, area percentages (for materials requiring two log-normal contributions), and numbers of particles counted are summarized in Table 2.

DISCUSSION

Morphology of the Carbon-Supported Ultrafine Metal Particles

The materials prepared using toluene possessed moderate to high surface areas, whereas the material prepared from neat $Fe(CO)_5$ had negligible surface area. The reasonably high surface area support would be sufficient for many catalytic applications. We have concluded that the moderate to high surface area carbonaceous matrix "support" was produced strictly from the toluene solvent and not from carbonyl remnants. The carbonyl remnants, however, did decompose to form a nonporous carbonaceous support of negligible surface area, as indicated by the Fe/nosol/Ar material.

Many metal/carbon materials prepared using laser photolysis or arc-discharge methods produce structures in which the metal particles serve as nucleation sites for the formation of carbon nanotubes and onion-like nanocapsules (62-68). In those studies, the metal particles were encapsulated by graphitic layers and are thus not accessible for catalysis. In the present study, with the exception of a few particles in the Fe/tol/Ar material (Figure 5), neither nanotube formation nor encapsulation by multiple graphitic layers was observed. Rather, the metal particles appeared to sit atop an amorphous carbon network. One possible explanation for the lack of graphitic metal encapsulation in our work compared with the complete encapsulation of metals in refs. 62-68 is

that graphene sheets are formed only when the plasma contains nearly pure carbon rather than the hydrogen-containing molecular (and free radical) species most surely produced by toluene dissociation. Different timescales for diffusion of reactant species may also have an important effect, as these materials are not equilibrium reaction products, but are metastable species produced by different (unknown) kinetically-limited growth mechanisms.

The Fe/tol/Ar material was the only material for which either graphitic encapsulation of metals or a bimodal metal particle size distribution was observed. It is probable that the bimodal particle size distribution for this material is related to the graphitic encapsulation, but no explanation for either of these phenomena can be provided at this time.

In all cases, the materials generated via microwave plasma decomposition of transition metal carbonyl compounds possessed mean metal particle sizes of less than 10 nm. The use of toluene to solvate the metal carbonyl precursors actually increased the mean metal particle size in the resulting "carbon-supported" metal particles. The addition of hydrogen to the argon carrier gas significantly decreased the mean particle size of the metal particles. Whether the hydrogen helped terminate growth of metal particles in the microwave plasma or kept the metal particles from agglomerating once on the carbonaceous surface remains unclear.

Several results from the mixed cobalt-molybdenum runs suggest that the overall particle formation process produced well-mixed particles at the atomic level. The lack of atomic number contrast in the TEM experiments indicated that 1) the particles had not segregated into Co-rich (light) and Mo-rich (dark) particles, 2) the surface segregation of the two metals was limited (which would make the outer surface of the particles unusually light or dark), and 3) the particles were not composed of smaller domains of Co and Mo (which would result in the particles appearing speckled). Finally, and most importantly, only $CoMoO_4$, an "atomically mixed" metal oxide, was observed in the bulk (Figure 7).

The finely-dispersed liquid droplets containing a few hundred to a few thousand molecules of the organometallic precursors drifted with the carrier gas and did not appear to agglomerate at the pressures used in our plasma experiments (~60 torr). We hypothesize that, as these droplets traversed the quartz-tubular reactor, most of the solvent was vaporized into the carrier gas. When the resulting, essentially dry, powders encountered the plasma boundary layer (3,000-5,000 K), they were instantaneously vaporized into their atomic species. As this vapor "cloud" remixed with the colder (500-800 K) bulk gas flowing around the plasma zone, the metal atoms rapidly condensed to produce the final metal particles. Thus, given a finite number of metal atoms contained in the individual powder particle, the dissociation kinetics within the plasma boundary layer and the condensation kinetics immediately outside would appear to control the particle size distribution. Further growth of the particles would be limited to agglomeration between particles exiting the plasma boundary layer. Larger particles consistent with such an agglomeration mechanism in this study were rare.

Particle Size Distributions

In all cases, the particle size distributions were best approximated by a log-normal distribution, rather than a simple normal distribution. Granqvist and Buhrman (3) have shown that the cumulative particle size distribution function $F_{LN}(x)$ corresponding to the probability density function described by Eq. 1 is given in Eq. 2.

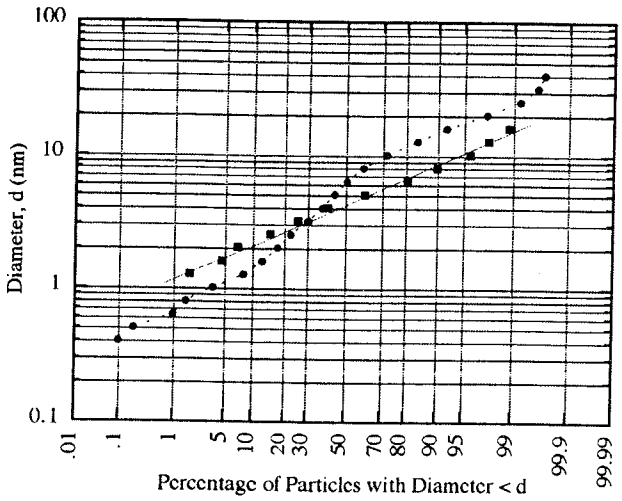

Figure 11. Cumulative particle size distribution plot for (●) Fe/tol/Ar and (■) Fe/nosol/Ar materials. For a particle size distribution which can be approximated with a single log-normal contribution, the fit is a straight line.

$$F_{LN}(x) = 0.5 + 0.5\,\mathrm{erf}\frac{\left[\ln(x/\bar{x})\right]}{\left[2^{0.5}\ln(\sigma)\right]} \qquad [2]$$

Thus, if one plots diameter (on a logarithmic scale) against the probability that a given particle is less than that diameter (a log-probability plot), for a particle size distribution which requires only one log-normal contribution, one should obtain a straight line (Figure 11). Significant curvature in a log-probability plot indicates either that additional log-normal contributions are required or that the log-normal distribution is inappropriate. It has been suggested by Villarica *et al.* (69) that there can be systematic deviations from linearity for log-normal particle size distributions without guaranteeing bimodality. We disagree with this assertion and note that Villarica *et al.* (69) base their assertion on time-of-flight mass spectrometry (TOF-MS) analysis of gas-phase clusters used to generate metal particles. The detection efficiency of TOF-MS is proportional to the number of atoms, introducing a systematic error into the size distribution which Villarica *et al.* have not corrected for.

From a log-probability plot, the log mean particle diameter corresponds to the diameter at 50% probability. In Eqs. 1 and 2, the geometric standard deviation, σ, is a dimensionless measure of the breadth of the particle size distribution and can be determined by dividing the diameter corresponding to 84.13% probability by the log mean diameter. As a result, the geometric standard deviation has a limit of 1.0 for infinitely sharp particle size distributions and is less than 2.0 except in extremely broad distributions. In general, the narrowest particle size distributions ($\sigma < 1.2$) correspond to an Ostwald ripening (atom addition) growth mechanism (3). Broader distributions indicate coalescence of small particles into larger particles. Clearly, coalescence growth is the dominant growth mechanism for the particles in this study.

10. Bernal, S., Botana, F.J., Calvino, J.J., Cauqui, M.A., Cifredo, G.A., Jobacho, A., Pintado, J.M., and Rodríguez-Izquierdo, J.M., *Journal of Physical Chemistry*, 1993, 97, 4118.
11. Lyman, C.E., Lakis, R.E., and Stenger, Jr., H.G., *Ultramicroscopy*, 1995, 58, 25.
12. Newcomb, S.B., Stobbs, W.M., and Little, J.A., *Physica Status Solidi A*, 1983, 76, 191.
13. Bi, X.-X., Ganguly, B., Huffman, G.P., Huggins, F.E., Endo, M., and Eklund, P.C., *Journal of Materials Research*, 1993, 8, 1666.
14. Rice, G.W., Fiato, R.A., and Soled, S.L., United States Patent 4,788,222, 1988.
15. Fiato, R.A., Rice, G.W., Miseo, S., and Soled, S.L., United States Patent 4,687,753, 1987.
16. Fiato, R.A., Rice, G.W., Miseo, S., and Soled, S.L., United States Patent 4,668,647, 1987.
17. Rao, V.U.S., *Energy & Fuels*, 1994, 8, 44.
18. Martino, A., Wilcoxon, J.P., and Kawola, J.S., *Energy & Fuels*, 1994, 8, 171.
19. Wilcoxon, J.P., United States Patent 5,147,841, 1992.
20. Moreno-Castilla, C., and Carrasco-Marín, F., *Journal of Chemical Society Faraday Transactions*, 1995, 91, 3519.
21. Rizzetti, A., Xhie, J., Sattler, K., Yamamoto, D., Pong, W., *Journal Elect. Spect. Rel. Phenom.*, 1992, 58, 359.
22. Dignard-Bailey, L., Trudeau, M.L., Joly, A., Schulz, R., Lalande, G., Guay, D., and Dodelet, J.P., *Journal of Materials Research*, 1994, 9, 3203.
23. Willwohl, H., Wolfrum, J., Zumbach, V., Albers, P., and Seibold, K., *Journal of Physical Chemistry*, 1994, 98, 2242.
24. Bentzon, M.D., Van Wonterghem, J., Mørup, S., Thõlèn, A., and Koch, C.J.W., *Philosophical Magazine B*, 1989, 60, 169.
25. Sawada, Y., Kageyama, Y., Iwata, M., and Tasaki, A., *Japanese Journal of Applied Physics*, 1992, 31, 3858.
26. Majima, T., Miyahara, T., Haneda, K., Ishii, T., and Takami, M., *Japanese Journal of Applied Physics*, 1994, 33, 4759.
27. Majima, T., Miyahara, T., Haneda, K., and Takami, M., Japan. *Japanese Journal of Applied Physics B*, 1994, 33, L225.
28. Majima, T., Miyahara, T., Haneda, K., and Takami, M., *Journal of Photochem. Photobiol. A*, 1994, 80, 423.
29. Zhao, X.Q., Zheng, F., Liang, Y., Hu, Z.Q., and Xu, Y.B., *Materials Letters*, 1994, 21, 285.
30. Jervis, T.R., and Zocco, T.G., *Materials Letters*, 1990, 9, 147.
31. Hayakawa, K., and Iwama, S., *Journal of Crystal Growth*, 1990, 99, 188.
32. Tasaki, A., Saegusa, N., and Oda, M., *IEEE Transactions Magnetics*, 1983, 19, 1731.
33. Gong, W., Li, H., Zhao, Z., Hadjipanayis, G.C., Kostikas, A., and Simopouos, A., *Journal of Applied Physics*, 1991, 70, 5900.
34. Gong, W., Li, H., Zhao, Z., and Chen, J., *Journal of Applied Physics*, 1991, 69, 5119.
35. Kusunoki, M., and Ichihashi, T., *Japanese Journal of Applied Physics*, 1986, 25, L219.
36. Hsu, C.-M., Lin, H.-M., Tsai, K.-R., and Lee, P.-Y., *Journal of Applied Physics*, 1994, 76, 4793.
37. Ohno, T., *Japanese Journal of Applied Physics A*, 1993, 32, 4648.
38. Moumen, N., Veillet, P., and Pileni, M.P., *Journal of Magnetism and Magnetic Materials*, 1995, 149, 67.
39. Furubayashi, T., Nakatani, I., and Saegusa, N., *Journal Physical Society Japan*, 1987, 56, 1855.
40. Chen, J.P., Sorensen, C.M., Klabunde, K.J., and Hadjipanayis, G.C., *Physics Review B*, 1995, 51, 11527.
41. Chou, C.-H., and Phillips, J., *Journal of Materials Research*, 1992, 7, 2107 .
42. Luborsky, F.E. and Lawrence, P.E., *Journal of Applied Physics*, 1961, 32, 231S.
43. Grinstaff, M.W., Cichowlas, A.A., Choe, S.-B., and Suslick, K.S., *Ultrasonics*, 1992, 30, 168.

44. Alphonse, P., Brieu, M., Gillet, M., and Mauret, P., *Journal de Chimie Physique*, 1988, 85, 669.
45. Windsor, C.G., Rainey, V.S., Rose, P.K., and Callen, V.M., *Journal of Physics F: Metal Physics*, 1984, 14, 1771.
46. Becker, J.A., Schäfer, R., Festag, R., Ruland, W., Wendorff, J.H., Pebler, J., Quaiser, S.A., Helbig, W., and Reetz, M.T., *Journal of Chemical Physics*, 1995, 103, 2520.
47. Cui, C.L., Dong, L.F., and Zhang, Z.K, *Nanostructured Materials*, 1995, 5, 829.
48. Jervis, T.R., and Newkirk, L.R., *Journal of Materials Research*, 1986, 1, 420.
49. Carver, G.E., Divrechy, A., Karbal, S., Robin, J., and Donnadieu, A., *Thin Solid Films*, 1982, 94, 269.
50. Chatterjee, A., and Chakravorty, D., *Applied Physics Letters*, 1992, 60, 136.
51. Kurihara, L.K., Chow, G.M., and Schoen, P.E., *Nanostructured Materials*, 1995, 5, 607.
52. Potapkin, B.V., Strelkova, M.I., Fridman, A.A., Harkness, J.B.L., and Doctor, R.D., in *Proceedings of the 12th International Symposium on Plasma Chemistry*, International Union of Pure and Applied Chemistry and the American Physical Society, Minneapolis, Minnesota, 1995.
53. Harkness, J.B.L., *Proceedings of the 29th Microwave Power Symposium*, International Microwave Power Institute, Chicago, Illinois, 1994.
54. International Centre for Diffraction Data, Card # 41-1487, Swarthmore, PA, 1995.
55. Brunauer, S., Deming, L.S., Deming, W.E., and Teller, E., *Journal of American Chemical Society*, 1940, 62, 1723.
56. Isirikyan, A.A., and Kiselev, A.V., *Journal of Physical Chemistry*, 1961, 65, 601.
57. Amberg, C.H., Spencer, W.B., and Beebe, R.A., *Canadian Journal of Chemistry*, 1955, 33, 305.
58. Halsey, G.D., Prenzlow, C.F., *Journal of Physical Chemistry*, 1957, 61, 1158.
59. International Centre for Diffraction Data, Card # 28-491, Swarthmore, PA, 1995.
60. International Centre for Diffraction Data, Card # 2-770, Swarthmore, PA, 1995.
61. International Centre for Diffraction Data, Card # 25-1434, Swarthmore, PA, 1995.
62. Seraphin, S., Wang, S., Zhou, D., and Jiao, J., *Chemical Physics Letters*, 1994, 228, 506.
63. Bethune, D.S., Kiang, C.-H., Goddard, W.A., Salem, J.R., and Beyers, R., *Journal of Physical Chemistry*, 1994, 98, 6612.
64. Ruoff, R.S., Lorents, D.C., Chan, B., Malhotra, R., and Subramoney, S., *Science*, 1993, 259, 346.
65. Bethune, D.S., Kiang, C.H., deVries, M.S., Gorman, G., Savoy, R., Vazquez, J., and Beyers, R., *Nature*, 1993, 363, 605.
66. Saito, Y., Yoshikawa, T., Okuda, M., Fujimoto, N., Sumiyama, K., Suzuki, K., Kasuya, A., and Nishina, Y., *Journal of Physical Chemistry of Solids*, 1993, 54, 1849.
67. Saito, Y., Yoshikawa, T., Okuda, M., Fujimoto, N., Yamamuro, S., Wakoh, K., Sumiyama, K., Suzuki, K., Kasuya, A., and Nishina, Y., *Chemical Physics Letters*, 1993, 212, 379.
68. Seraphin, S., Zhou, D., Jiao, J., Minke, M.A., Wang, S., Yadav, T., and Withers, J.C., *Chemical Physics Letters*, 1994, 217, 191.
69. Chaiken, J., Casey, M.J., and Villarica, M., *Journal of Physical Chemistry*, 1992, 96, 3183.